Towards high-quality multi-spot-welded joints in thermoplastic composite structures

Zhao, Tian; Palardy, Genevieve; Villegas, Irene F.; Benedictus, Rinze

Publication date
2017

Document Version
Final published version

Published in
21st International Conference on Composite Materials, ICCM 2017

TOWARDS HIGH-QUALITY MULTI-SPOT-WELDED JOINTS IN THERMOPLASTIC COMPOSITE STRUCTURES

Tian Zhao[1], Genevieve Palardy[1], Irene F. Villegas[1] and Rinze Benetictus[1]

[1] Structural Integrity & Composites Research Group, Faculty of Aerospace Engineering, Delft University of Technology, Kluyverweg 1, 2629HS, Delft, the Netherlands
Emails: T.Zhao@tudelft.nl, G.Palardy@tudelft.nl, I.FernandezVillegas@tudelft.nl, and R.Benedictus@tudelft.nl

Keywords: Thermoplastic composites, Ultrasonic spot welding, Welding process control, Mechanical behaviour, Fracture analysis

ABSTRACT

Ultrasonic welding is a promising assembly technique for thermoplastic composites and it is well-suited for spot welding. In this study, two typical welding process control strategies, i.e. displacement-controlled and energy-controlled welding, were selected to manufacture spot-welded joints. The influence of different boundary conditions, provided by different welding jigs, on the welding process and the performance of thus-created welded joints were investigated. The optimum input energy was found dependent on the welding jigs, while the optimum displacement was consistent for achieving the maximum weld strength in both welding jigs. Therefore, displacement-controlled welding showed more potential in producing consistent welds in sequential multi-spot welding.

1 INTRODUCTION

Thermoplastic composites (TPCs) are becoming increasingly attractive for their use in aircraft structures owing to their high-grade mechanical properties compared to metallic materials and to their cost-effective manufacturing process compared to thermoset composites (TSCs) [1-3]. Since thermoplastic polymers can be melted when heated to a certain temperature and recover their initial properties after cooling down, TPCs can be welded. Ultrasonic welding is a very interesting technique for joining TPCs with advantages such as short welding time, absence of foreign materials in the weldline and possibility for in-situ process monitoring [1, 4, 5]. In addition, benefitting from the high energy concentration, ultrasonic welding is well-suited for manufacturing spot-welded (SW) joints. Although ultrasonic spot welding has been extensively investigated and industrially applied for the conventional metallic materials and their alloys [6-8], the knowledge of its application in TPCs is still very limited. The development of robust welding procedures is deemed necessary for manufacturing SW joints with consistent quality, which can be a promising solution for the assembly of mass-produced parts such as clips and brackets in composite aircraft or automotive structures.

Ultrasonic welding procedures are usually controlled based on three modes, e.g. time, energy and vertical displacement of the sonotrode. These modes have been applied and investigated in the literature on manufacturing of TPC welded joints [4, 9-11]. An experimental investigation was carried out by Harras [6] on the optimization of the ultrasonic welding of carbon fibre reinforced polyetheretherketone (CF/PEEK) composites. He found the optimum welding time (i.e. the welding time resulting in maximum critical strain energy release rates) had a significant dependence on the sample configuration being welded. However, the fracture toughness of welded joints was reported to show a good correlation to the total energy input. Villegas [4] proposed a methodological approach to determine the optimum weld strength of carbon fibre reinforced polyetherimide (CF/PEI) composites based on the process output data, i.e. dissipated power and displacement of the sonotrode. In addition, a comparison of the relationship between lap-shear strength (LSS) of welded joints and sonotrode displacement, welding energy and vibration time, was carried out. The results indirectly indicated that, compared to vibration time and welding energy, welds with consistent quality were more likely to be produced with a fixed sonotrode displacement value even in different welding conditions, such as

welding force and vibration amplitude. However, neither energy-controlled nor time-controlled welding was performed in this research. In the research recently published by Zhao [11], ultrasonic spot-welded joints were successfully created with energy-controlled process and excellent in-plane mechanical performance was obtained when compared to mechanically fastened joints. However, according to the research in [12], the input energy was not only used to create welds, but also dissipated in the adherends, the fixture and the base during the welding process. Therefore, different energy is expected to be required for creating consistently high-strength welds if the welding conditions, e.g. boundary conditions, are changed. On the contrary, the displacement of the sonotrode is predominantly related to the physical changes at the weldline, which is independent of the energy dissipated in the surroundings [4], and hence, is more likely insensitive to changes in welding conditions.

This paper mainly focuses on the impact of changes in boundary conditions on two different ultrasonic welding process control strategies, i.e. energy-controlled and displacement-controlled welding, in CF/PPS (carbon fibre reinforced polyphenylene sulfide) thermoplastic composites. Two different welding jigs were employed to introduce the different boundary conditions. The welding process was analysed through the output data, i.e. power and displacement curves provided by the ultrasonic welder. The quality of the SW joints was evaluated by mechanical testing and fractography analysis.

2 EXPERIMENTAL

2.1 Materials

Panels, with a stacking sequence of $[(0/90)]_{3S}$, were made of 6 layers of 5 harness satin powder-impregnated CF/PPS prepregs, supplied by Ten Cate Advanced Composites in The Netherlands. The laminates were consolidated in a hot platen press at 320°C and 1 MPa for 20 min. Adherends of 101.6 x 25.4 mm^2 were cut by a water-cooled diamond saw and welded in a single-lap configuration with a 25.4 x 25.4 mm^2 square overlap, as shown in Figure 1. Spot-welded joints were created in the central point of the overlap with 4 mm-diameter-circular energy directors (EDs). The EDs were manually fixed on the bottom adherend prior to the welding process.

2.2 Welding process

A 20 kHz Rinco Dynamic micro-processor controlled ultrasonic welder was used in this study to weld individual samples. Based on the previous research in [11], a 10 mm-diameter-circular sonotrode was employed to manufacture SW joints. Two different welding jigs, namely Jig Z51414 and Jig 9109 (see Figure 2), were utilized to provide different boundary conditions for the welding process. For clarity, Jig Z51414 and Jig 9109 were hereafter denoted as Jig 1 and Jig 2 in the paper and further simplified as J1 and J2 in the samples names, respectively. Both top and bottom adherends were bar clamped in Jig 1 and hence only the top part of the overlap could move during the vibration phase. In contrast, the top adherend in Jig 2 was clamped in a sliding platform, which allowed a vertical movement for the entire adherend throughout the welding process.

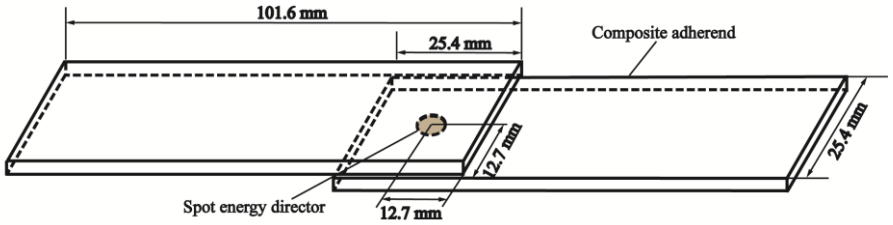

Figure 1: Schematic of the configuration of single-lap spot-welded joints. The grey dashed ellipses indicate the spot energy directors. Dimensions are not to scale.

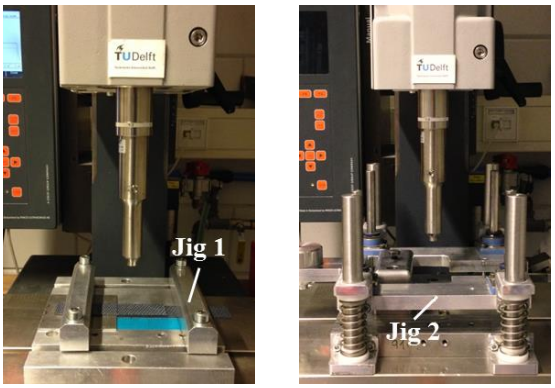

Figure 2: Ultrasonic welder, circular sonotrode and clamping jigs used in this study.

Based on the results in [11], a vibration amplitude of 60.8 μm (peak-to-peak) and a welding force of 1500 N, were used in this work. During the vibration stage, the welding force was increased at a rate of 1000 N/s in both displacement-controlled and energy-controlled processes. The solidification force and time were respectively set to 1500 N and 4 s. The optimum input displacement and energy were identified based on the methodology proposed by Villegas in [4]. According to the statement, the vibration phase can be basically divided into 5 stages and the maximum weld strength is consistently obtained in stage 4. Therefore, the corresponding displacement and energy input are defined as the optimum input values.

2.3 Testing and characterization

The single-lap welded joints were mechanically tested in a Zwick/Roell 250 KN universal testing machine with a crosshead speed of 1.3 mm/min, following the ASTM D1002 standard. In this study, lap-shear strength (LSS) was selected to characterize the mechanical behaviour of SW joints, which was calculated as ultimate failure load (UFL) divided by the final welded area (WA) of welded joints. The UFL was reported as the maximum load achieved during the tests. The WA of welded joints was measured with ImageJ150 software (NIH) based on the fracture surfaces captured by a Zeiss Stereo-microscope. Finally, failure modes of SW joints were analysed by a JEOL JSM-7500F Scanning Electronic Microscope (SEM).

3 RESULTS AND DISCUSSION

3.1 Welding output curves

Figure 3 and 4 illustrate the optimum sonotrode displacement and welding energy identified from the power curves for both welding jigs. It must be noted that the same optimum displacement value, 0.25 mm, was consistently obtained even when different welding jigs were used. Given 0.25 mm sonotrode displacement, power curves reached stage 4 of the vibration phase for both cases (see Figure 3). On the contrary, the optimum welding energy was noted as approximately 420 J and 350 J for Jig 1 and Jig 2, respectively. This change in the optimum welding energy due to different boundary conditions entails that, in sequential multi-spot welded joints, each weld needs different optimum welding energy values.

3.2 Mechanical behaviour

Lap-shear strength, accompanied by the corresponding ultimate failure load (UFL) and final welded area (WA), of SW joints welded at the optimum sonotrode displacement and welding energy in both welding jigs are summarized in Figure 5. In addition, as a comparative study, samples welded at 350 J energy in Jig 1 and at 420 J in Jig 2 were also mechanically tested and the results are shown in Figure 5 as well, indicated by $J_1/E_{<opt}$ and $J_2/E_{>opt}$, respectively. The error bars stand for the standard deviations. As depicted in Figure 5(a), LSS of all samples studied in the experiments displays

comparable values, ranging from 36 MPa to 38 MPa. Considering the similar LSS of approximately 38 MPa achieved by the welded joints created with flat EDs in [10], it can be noted that both displacement-controlled and energy-controlled process are likely to create high-strength welds. Even given the lower input energy in $J_1/E_{<opt}$ joints, LSS still shows similar values to the samples welded at the optimum energy. All the samples show low scatter in LSS, below 4 %, except for the samples created at 420 J in Jig 2 (approximately 7%). This scatter is likely the result of over-welding, which is explained in the fracture analysis in Section 3.3.

The average final WA of the samples is shown as a percentage of the original area of the ED (see Figure 5(b)). Therefore, the squeeze-flow of the molten EDs during the process can be clearly indicated. Given the same welding jig, the difference between samples welded with displacement and energy is comparable, approximately 8%. This is correlated with the difference in the UFL of the corresponding joints. An obvious drop in the final welded area, as well as the UFL, is found in the sample welded at 350 J in Jig 1. This should be attributed to the lower energy (compared to the optimum value) resulting in a lower welding time and thus creating a smaller welded area.

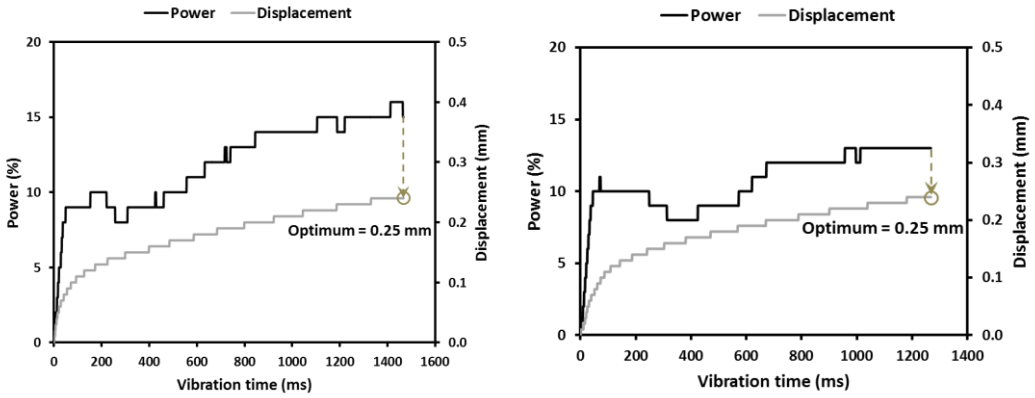

(a) (b)

Figure 3: Representative power and displacement curves for SW joints welded at 0.25 mm displacement in Jig 1 (a) and Jig 2 (b).

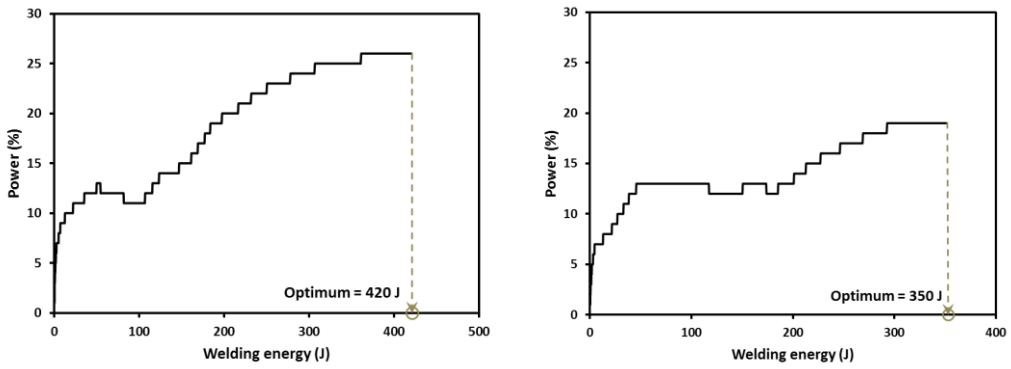

(a) (b)

Figure 4: Representative power and displacement curves for SW joints welded at 420 J energy in Jig 1 (a) and at 350 J in Jig 2 (b).

.

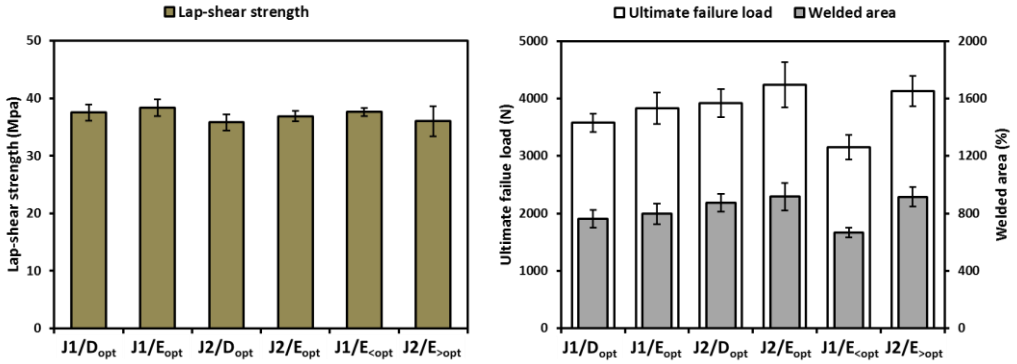

(a) (b)

Figure 5: Ultimate failure load, welded area (a) and calculated lap-shear strength (b) of SW joints manufactured with displacement-controlled and energy-controlled welding in combination with different welding jigs.

3.3 Failure mode analysis

Fractography was carried out on the fracture surfaces of the mechanically tested SW joints to analyse the failure modes. As shown in Figure 6, intralaminar failure is found to be the predominant failure mode of the SW joints manufactured at the optimum input in both displacement-controlled and energy-controlled welding. The main characteristic features are debonding of fibre and matrix, presenting as bare fibres and deep fibre imprints on the thermoplastic resin, accompanied by fibre breakage. This failure mode indicates that high quality joints are created by the welding process [13]. Different from that, the fracture surfaces of joints welded at 350 J in Jig 1 are mainly characterized by a resin-rich area, together with partially debonded fibres covered by resin cusps (see Figure 7 (a)). The fibre imprints are not as deep as in the joints created at the optimum energy. In contrast, significant void imprints formed in the thermoplastic matrix demonstrate the samples are over-welded in the condition of 420 J in Jig 2 (see Figure 7 (b)). The formation of porosities at the weldline is likely the cause of high scatter in the LSS of $J_2/E_{>opt}$ joints (see Figure 5(a)). Moreover, the variations of fracture modes found in the SW joints created at the non-optimum energy confirm that the definition of the optimum welding energy is dependent on the usage of the welding jigs, i.e. boundary conditions.

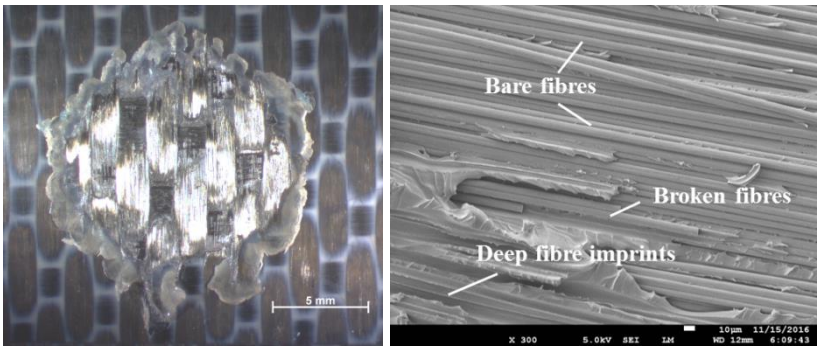

Figure 6: Representative fracture surfaces (left) and SEM micrographs (right) of the SW joint welded at the optimum input displacement or energy. The scale bars are 5 mm (for stereo-microscopy) and 10 μm (for SEM).

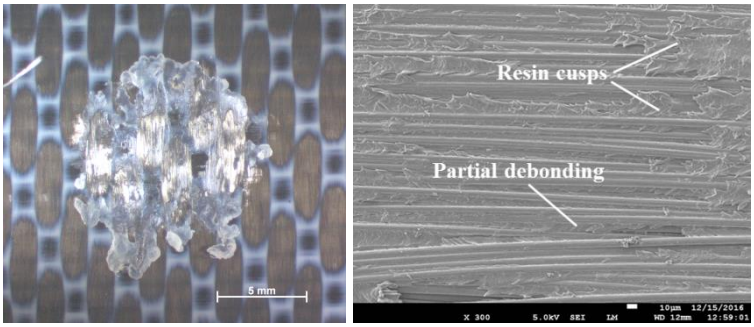

(a)

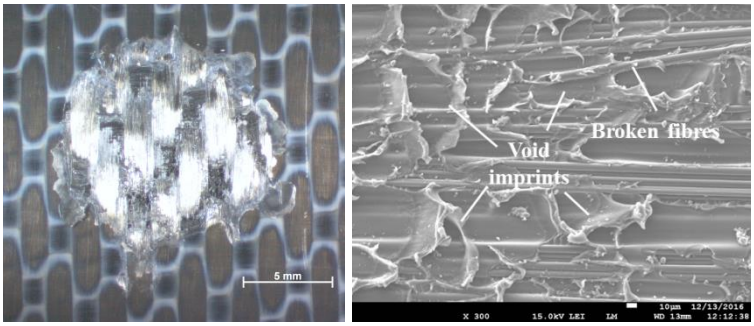

(b)

Figure 7: Representative fracture surfaces (left) and SEM micrographs (right) of the SW joint welded at 350 J energy in Jig 1 (a) and at 420 J energy in Jig 2 (b). The scale bars are 5 mm (for stereo-microscopy) and 10 μm (for SEM).

3.4 Further outlooks on multi-spot welding

Based on the experimental results presented above, the optimum sonotrode displacement showed an independence to different boudary conditions. Therefore, multi-spot welded (MSW) joints, formed by two single-spot welds were manufactured by using the displacement-controlled welding. Figure 8 shows a respresentative fracture surface of both welds created in the MSW joint. Both welds are found to be of similar size and the fracture surfaces are consistent with each other. The SEM micrographs report that intralaminar failure is the predominant failure mode for both welds, similar to the findings in the single-spot joints created by displacement-controlled welding in the previous section. This observation also implies that displacement-controlled welding is an appropriate process control for sequential multi-spot welding.

4 CONCLUSIONS

A detailed experimental investigation, including manufacturing and mechanical testing, was carried out to study the impact of changes in boundary conditions on two welding process control strategies: displacement-controlled and energy-controlled welding. Based on the experimental results, the following conclusions can be drawn:

- Different welding energy values were required for achieving the maximum weld strength of the spot-welded (SW) joints when different welding jigs were used. In contrast, the optimum sonotrode displacement was found to be the same for both jigs, which indicated that displacement-controlled welding was less sensitive to the influence of change in boundary conditions.
- Given the optimum sonotrode displacement and energy, high-strength welds could be obtained by both types of welding process. Furthermore, intralaminar failure, featured by fibre-matrix debonding and fibre breakage, was found to be the predominant failure mode in the SW joints.
- Displacement-controlled welding was applied for manufacturing MSW joints. Consistent welds, i.e. similar size and failure mode, were obtained for both welds in the MSW joints, indicating that the displacement-controlled welding was a reliable and promising technique for sequential multi-spot welding of larger composite structures.

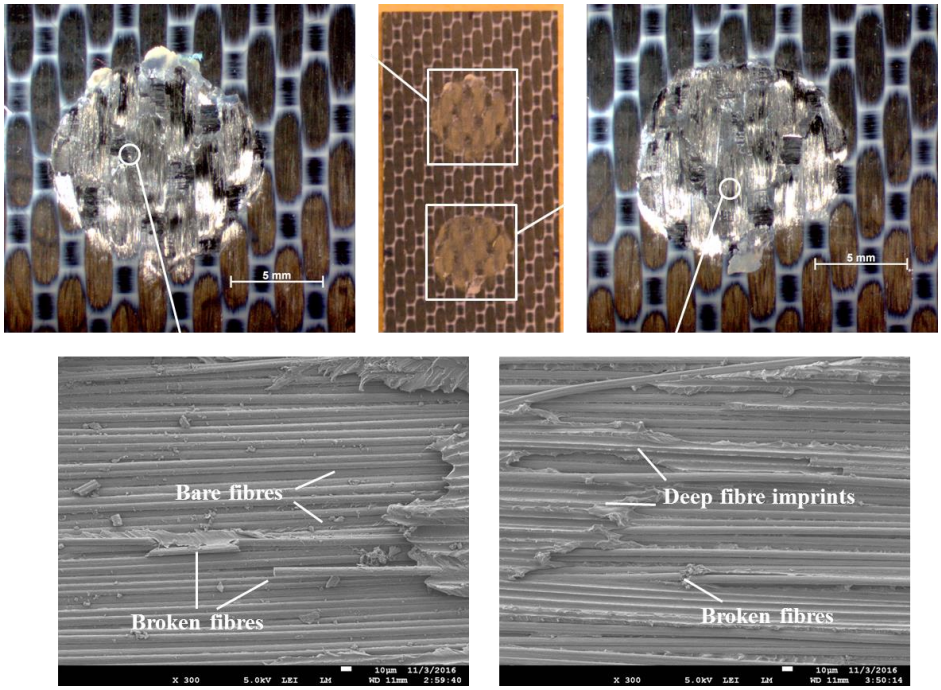

Figure 8: Representative fracture surfaces (middle) of the MSW joints manufactured with displacement-controlled welding at 0.25 mm displacement. The scale bars are 5 mm (for stereo-microscopy) and 10 μm (for SEM).

ACKNOWLEDGEMENTS

T. Zhao thanks the PhD Scholarship Fund from China Scholarship Council (CSC) for overseas study.

REFERENCES

[1] C. Ageorges, L. Ye and M. Hou, Advances in fusion bonding techniques for joining thermoplastic matrix composites a review, *Composites Part A: Applied Science and Manufacturing*, **32**, 2001, pp. 839-857.

[2] A. Yousefpour, M. Hojjati and J.P. Immarigeon. Fusion bonding/welding of thermoplastic composites, *Journal of Thermoplastic composites Materials*, **17**, 2004, pp. 303-341.

[3] H. Shi, I.F. Villegas and H.E.N. Bersee. Strength and failure modes in resistance welded thermoplastic composite joints: Effect of fibre–matrix adhesion and fibre orientation. *Composites Part A: Applied Science and Manufacturing*, **55**, 2013, pp. 1-10.

[4] I.F. Villegas. Strength development versus process data in ultrasonic welding of thermoplastic composites with flat energy directors and its application to the definition of optimum processing parameters. *Composites Part A: Applied Science and Manufacturing*, **65**, 2014, pp. 27-37.

[5] I.F. Villegas. In situ monitoring of ultrasonic welding of thermoplastic composites through power and displacement data. *Journal of Thermoplastic Composite Materials*, **28(1)**, 2013, pp. 66-85.

[6] V.K. Patel, S.D. Bhole and D.L. Chen. Ultrasonic spot welding of lightweight alloys, *Proceeding of 13th International Conference on Fracture, Beijing, China, June 16-21, 2013*, pp. 1-10.

[7] A. Macwan, V.K. Patel, X.Q. Jiang, C. Li, S.D. Bhole and D.L. Chen. Ultrasonic spot welding of Al/Mg/Al tri-layered clad sheets, *Materials and Design*, **62**, 2014, pp. 344-351.

[8] P. Prangnell, F. Haddadi and Y. C. Chen. Ultrasonic spot welding of aluminium to steel for automotive applications-microstructure and optimisation, *Materials Science and Technology*, **27(3)**, 2011, pp. 613-624.

[9] B. Harras, K.C. Cole and T. Vu-Khanh. Optimization of USW of PEEK-carbon composites. *Journal of Reinforced Plastics and Composites*, **15**, 1996, pp. 174-182.

[10] I.F. Villegas, B.V. Grande, H.E.N. Bersee and R. Benedictus. A comparative evaluation between flat and traditional energy directors for ultrasonic welding of CF/PPS thermoplastic composites, *Composite Interfaces*, **22(8)**, 2015, pp. 717-729.

[11] T. Zhao, G. Palardy, I.F. Villegas, C. Rans, M. Martinez and R. Benedictus. Mechanical behaviour of thermoplastic composites spot-welded and mechanically fastened joints: A preliminary comparison. *Composites Part B: Engineering*, 112, 2017, pp. 224-234.

[12] A. Benatar and T.G. Gutowski. Ultrasonic Welding of PEEK Graphite APC-2 Composites. *Polymer enegineering and science*, **29**, 1989, pp. 1705-1721.

[13] I.F. Villegas and H.E.N. Bersee. Ultrasonic welding of advanced thermoplastic composites: An investigation on energy-directing surfaces. *Advances in Polymer Technology*, **29(2)**, 2010, pp. 112-121.